Advanced Techniques for Evaluating Trunk Health: Integrating 3D Photogrammetry with Dual-polarized GPR Survey

Lilong Zou
Faculty of Engineering, Computing and the Environment
Kingston University
London, UK
l.zou@kingston.ac.uk

Ying Li
School of Computing and Mathematical Sciences
Birkbeck, University of London
London, UK
ying.li1@bbk.ac.uk

Kevin Munisami
Faculty of Engineering, Computing and the Environment
Kingston University
London, UK
j.munisami@kingston.ac.uk

Amir M. Alani
Faculty of Engineering, Computing and the Environment
Kingston University
London, UK
m.alani@kingston.ac.uk

***Abstract*—The importance of forests is emphasized through their roles in climate regulation, soil and water conservation, and biodiversity support. Sustainable forest management is promoted for its long-term benefits, though challenges such as tree diseases pose risks to safety, property, and cultural values, causing economic losses. Traditional invasive inspection methods have been supplemented by non-destructive techniques like ground-penetrating radar (GPR). However, accurate disease detection is hindered by tree structures and electromagnetic complexities. To address this, a method combining structure-from-motion photogrammetry with dual-polarized GPR survey has been proposed. Enhanced algorithms mitigate irregular shapes, improving precision and efficiency in disease monitoring.**

Keywords—Ground Penetrating Radar (GPR), tree trunk inspection, structure-from-motion (SfM) photogrammetry, Dual-polarized radar

I. INTRODUCTION

Forests play a critical role in maintaining global ecosystem stability by regulating the climate, supporting biodiversity, and supplying essential resources such as timber, fuel, and non-timber forest products. They act as carbon sinks, helping to mitigate climate change, and serve as natural barriers that reduce the impact of natural disasters like floods and landslides. Additionally, forests purify the air, filter water, and provide noise reduction, enhancing overall environmental quality and human well-being. The preservation of forest health is especially important, as natural forests can take decades or even centuries to mature, and existing trees are increasingly threatened by pests, diseases, and the impacts of climate change. In urban areas, deteriorating or decaying trees pose risks to public safety and property, making proactive tree management essential. This includes monitoring the health of culturally and ecologically significant ancient trees. Sustaining forest health supports ecosystems, safeguards economies, and ensures the longevity of vital natural services.

Tree diseases frequently begin deep within the trunk, gradually expanding outward and leading to internal decay or the formation of cavities that compromise the tree's structural integrity. These internal issues are often invisible from the outside, making early detection both crucial and challenging. Traditional inspection methods, such as resistance drilling, involve penetrating the trunk to assess its internal condition. However, these invasive techniques can be detrimental, as they create wounds that serve as potential entry points for harmful pathogens, ultimately worsening the health condition of trees. In response to these limitations, non-destructive testing (NDT) methods like acoustic tomography, electrical resistance measurements, and X-ray imaging have been developed. Although these techniques offer valuable insights without causing physical harm, they often come with significant drawbacks, including high costs, complex operational requirements, and limited effectiveness in certain environmental or structural conditions. Ground Penetrating Radar (GPR) has emerged as a promising alternative for identifying internal decay and hollow sections in trees. It works by emitting electromagnetic waves that reflect off internal anomalies. However, the effectiveness of GPR is hindered by factors such as the irregular geometry of tree trunks and the variable electromagnetic properties of wood, which complicate signal interpretation and reduce detection accuracy. Further research and technological refinement are needed to fully harness the potential for tree health diagnostics with GPR surveys.

This study introduces an innovative framework that integrates Structure-from-Motion (SfM) photogrammetry with dual-polarized GPR techniques to address longstanding limitations in tree health monitoring. By leveraging SfM, the approach generates high-accuracy 3D reconstructions of tree trunks, which significantly improves the interpolation of GPR tracks around complex geometries. This allows for more precise detection of internal anomalies, such as decay or cavities. To further enhance the quality of subsurface imaging, a novel signal processing strategy incorporating dual-polarization reflections is implemented, effectively increasing both data accuracy and signal-to-noise ratios (SNR). Additionally, the use of an arc-shaped Kirchhoff migration algorithm helps correct distortions caused by irregular trunk shapes, thus ensuring more reliable interpretation of GPR data. The framework was validated through real-world testing, successfully identifying early stages of internal decay—critical for enabling timely intervention. This non-invasive,

efficient method has significant implications for forest and urban tree management, aiding biodiversity preservation and supporting long-term ecosystem sustainability by facilitating proactive health assessments.

II. Methodology

A. SfM Photogrammetry Technique

To address the challenges posed by the irregular geometry of tree trunks, this study utilizes the SfM photogrammetry technique to precisely determine the survey position of each GPR trace. SfM operates on a principle akin to modern camera systems that stitch overlapping photographs into a seamless 2D panorama [1]. The process involves estimating an optimal set of camera parameters and 3D coordinates to minimize reprojection errors across all captured images and feature points while imposing constraints on the reconstructed 3D structure, as illustrated in Figure 1. By analyzing the movement of camera through three-dimensional space, SfM calculates the X, Y, and Z coordinates of each pixel from the original images, generating detailed 3D models of the tree trunk. As a non-linear, non-convex optimization problem, SfM requires iterative computational techniques for accurate solution derivation. In this study, a single camera was used to capture images and generate a 3D Digital Elevation Model (DEM) of the surveyed tree trunk. The accuracy of SfM with a single camera depends largely on the amount of camera movement, the quality of feature detection, and the ability to address challenges related to scale ambiguity and depth estimation. A pre-measured true dimension can be used to determine the scale factor, allowing single-camera SfM to achieve sub-centimeter accuracy [2].

Figure 2 shows a processing flowchart that builds a 3-D DEM of the tree trunk and extracts a GPR survey trace. In this study, we employed a single-camera setup to capture images and construct a 3D DEM of the surveyed tree trunk using SfM photogrammetry. While this method offers notable cost and portability advantages over multi-camera systems or advanced 3D scanners, it presents several challenges. Accurate reconstruction depends heavily on sufficient camera motion, effective feature detection, and addressing scale ambiguity. Environmental factors such as lighting variations and occlusions can reduce feature matching reliability, negatively affecting model accuracy. Moreover, single-camera SfM cannot inherently determine real-world scale without additional references like GPS data or known landmarks. Depth estimation also becomes less accurate with increasing distance, particularly in outdoor settings or scenes with

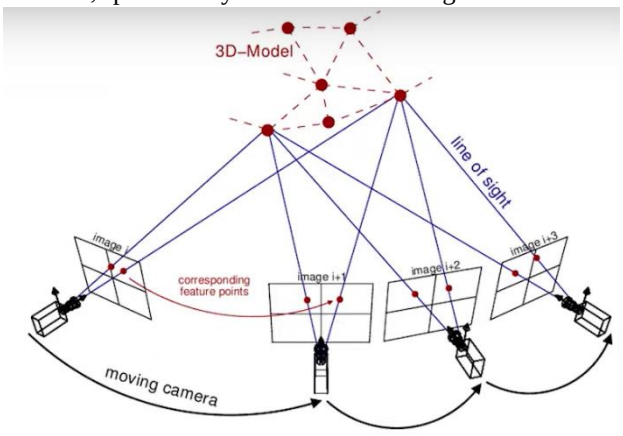

Fig. 1. 3D geometric reconstruction using SfM technique.

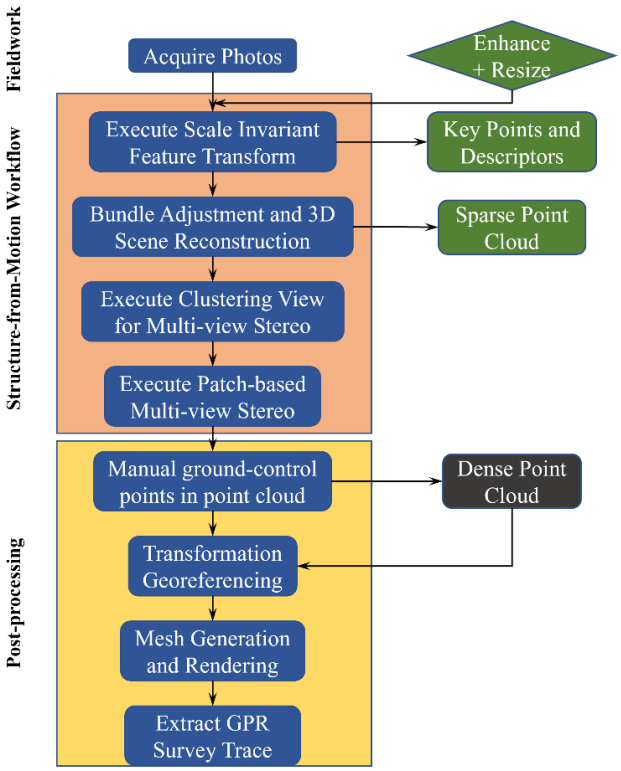

Fig. 2. Flow chart building 3D DEM of tree trunk and extracting GPR survey trace.

repetitive structures. Despite these limitations, single-camera SfM can achieve sub-centimeter accuracy in controlled conditions—far exceeding the resolution of GPR systems. This high precision enables accurate alignment of GPR traces with the 3D model, enhancing subsurface imaging and improving anomaly interpretation.

B. Holographic Radar Tomography

Recovering the relative permittivity from GPR data is considered crucial for interpreting subsurface materials. The first use of dual-polarization reflections to estimate the Martian surface relative permittivity was introduced in [3]. In this paper, this method is extended to estimate the subsurface relative permittivity (not only the surface) using the dual polarization response. The signal-to-noise ratio is significantly enhanced by fusing HH and VV reflections with the proposed approach.

Figure 3 illustrates the behavior of an electromagnetic wave as it travels from the GPR transmitter antenna into the tree trunk. The interaction of the wave with the medium is governed by Maxwell equations, leading to the generation of scattered fields. These fields are influenced by the frequency-dependent reflection and transmission properties of the medium, which are described by its global reflection and transmission coefficients [4]. The resulting scattered fields are determined by these coefficients, which are shaped by the design of the antenna and the characteristics of the reflected signals [5]. When the same antenna functions as both the transmitter and receiver in HH and VV polarization modes, the frequency-domain relationship between the radar-detected fields for these modes can be expressed as follows:

$$S_{HH}(\omega) = \frac{B_{HH}(\omega)}{A_{HH}(\omega)} = R_{HH}(\omega) + T^{i}_{HH}(\omega)\mathcal{F}_{HH}(\omega)T^{s}_{HH} \quad (1)$$

$$S_{VV}(\omega) = \frac{B_{VV}(\omega)}{A_{VV}(\omega)} = R_{VV}(\omega) + T_{VV}^{i}(\omega)\mathcal{F}_{VV}(\omega)T_{VV}^{s} \quad (2)$$

The HH and VV reflected signals, denoted as $S_{HH}(\omega)$ and $S_{VV}(\omega)$, represent the responses in their respective polarization modes. These signals are calculated as the ratio of the backscattered field $B(\omega)$ to the incident field $A(\omega)$ at the GPR reference plane, with ω representing angular frequency. The parameters $R_{HH}(\omega)$ and $R_{VV}(\omega)$ correspond to the overall reflection coefficients for the radar system, capturing the direct coupling between the transmitter and receiver in HH and VV modes. The antenna characteristics are described by T^{i}, the transmitter coefficient for the incident field at the reference plane, and T^{s}, the receiver coefficient for the reflected field returning to the radar. The scattering properties of the target are represented by the scattering coefficient $\mathcal{F}(\omega)$, which is defined mathematically as follows:

$$\mathcal{F}_{HH}(\omega) = \mathcal{L}_{HH}(\omega)\varepsilon_{target} \quad (2)$$

$$\mathcal{F}_{VV}(\omega) = \mathcal{L}_{VV}(\omega)\varepsilon_{target} \quad (3)$$

Here, $\mathcal{L}$ represents the scattering loss factor, while ε_{target} denotes the overall relative permittivity of target. The scattering loss factor, $\mathcal{L}(\omega)$, is influenced by a range of physical attributes, such as the dimensions, geometry, and material composition of target. Its formulation can be expanded to reflect these dependencies as follows:

$$\mathcal{L}(\omega) = f(\sigma, \lambda, \varepsilon_{target}) \quad (4)$$

where σ is the conductivity of the target. λ is the wavelength of the incident wave.

Because the direct antenna coupling is a constant value, it can be eliminated by subtracting the radar measurement obtained in free space. As a result, Eqs. (1) and (2) can be reformulated as:

$$S'_{HH}(\omega) = T_{HH}^{i}(\omega)\mathcal{F}_{HH}(\omega)T_{HH}^{s} \quad (5)$$

$$S'_{VV}(\omega) = T_{VV}^{i}(\omega)\mathcal{F}_{VV}(\omega)T_{VV}^{s} \quad (6)$$

Assume that $T_{HH}^{i} = T_{HH}^{s} = T_{VV}^{i} = T_{VV}^{s}$, indicating that the antenna coefficients for both HH and VV polarization modes are treated as equivalent. With this assumption, the framework for the proposed holographic radar tomography can be expressed as follows:

$$\frac{S'_{HH}(\omega)+S'_{VV}(\omega)}{1+\frac{S'_{VV}(\omega)}{S'_{HH}(\omega)}} + \frac{S'_{HH}(\omega)-S'_{VV}(\omega)}{1-\frac{S'_{VV}(\omega)}{S'_{HH}(\omega)}} = \Gamma \cdot \varepsilon_{target} \quad (7)$$

Here, Γ represents a real-valued scaling factor that accounts for both scattering losses and the characteristics of antenna. Following this adjustment, the GPR profile is scaled and mapped to the relative permittivity, ε_{target}, by applying the factor Γ.

III. Measurement and Results

A. Dual-polarized GPR and Field Survey

This study utilizes the advanced capabilities of the compact dual-polarized "Aladdin" GPR system, developed by IDS GeoRadar, a division of Hexagon (see Figure 3). The Aladdin system features two 2 GHz antennas arranged perpendicularly, operating in HH and VV polarization channels. This dual-polarized setup allows for the simultaneous collection of polarimetric data, offering a more detailed and comprehensive view of subsurface structures [35].

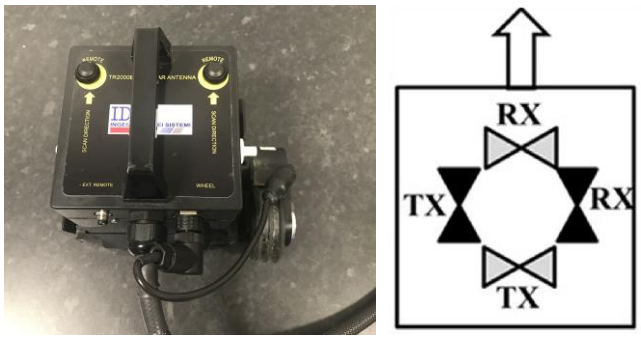

Fig. 3. Dual-polarized "Aladdin" Ground Penetrating Radar system and antenna configuration.

As illustrated in Figure 3, the perpendicular antenna configuration is essential for accurately capturing polarized signals. One of the key advantages of this configuration is its improved depth penetration, achieved through the combined analysis of both HH and VV channels. This dual-polarization capability enables the system to detect both shallow and deeper anomalies with enhanced clarity. Such performance is especially beneficial in applications requiring high-resolution subsurface imaging, making the Aladdin GPR system a critical component of the tree health monitoring approach presented in this study.

A field inspection was carried out on a living tree located in Walpole Park, London, UK. Based on the bark's color and the overall health condition observed during the inspection, the tree was preliminarily diagnosed as being affected by disease. The tree measured approximately 15 meters in height, with a trunk radius of about 40 centimeters. For detailed analysis, a total of 132 photographs were captured using a Canon EOS camera equipped with an 18 mm fixed focal length lens. These images were taken from a variety of angles and distances to ensure comprehensive coverage, forming the basis for an accurate 3D DEM reconstruction. During the GPR survey, three circle strings spaced at 20 cm intervals were installed, aiding in the calculation of the scale factor, which is essential for subsequent data analysis.

After acquiring the detailed 3D geometry of the tree trunk, the next step involves extracting the cross-sectional outline of trunk at the exact height corresponding to the GPR survey traces. To achieve this, 21 individual GPR scans are performed, each spaced 2 cm apart. In the Figure 4, blue circles represent the locations of the GPR survey traces, while red stars denote the starting points of each trace. This uniform spacing guarantees an even distribution of measurements around the trunk's circumference, enabling full coverage of the cross-section. Such precision in positioning enhances the reliability and resolution of the internal structural data obtained from the GPR scans. The method ensures that no part of the cross-section is overlooked, providing a robust dataset for subsequent analysis of internal anomalies or decay patterns within the tree trunk.

The 3D geometry of the tree trunk, captured with sub-centimeter precision, provides spatial accuracy far exceeding the resolution of the dual-polarized GPR system. This level of detail allows each GPR trace to be precisely aligned with the surface of trunk, greatly improving the accuracy of subsurface imaging. Such precision is especially important

for tree trunk inspection, where accurate mapping of internal anomalies—such as decay or voids—must be related directly to the external structure. Aligning GPR data with a highly detailed surface model enables better identification of structurally vulnerable areas that may otherwise go unnoticed. This integrated approach significantly enhances the reliability of GPR-based analysis and represents a major advancement in the study of tree health. By combining high-resolution 3D models with GPR data, researchers are now able to explore the internal architecture of trees with a new level of clarity, supporting early detection of decay and improved management of tree health.

B. *Data processing*

1) Pre-processing: Before analyzing the data, a comprehensive pre-processing stage was performed to minimize unwanted reflections and enhance the signal-to-clutter ratio. This process involved three key steps: First, a time-zero adjustment was applied to align all traces with the critical moment the radar signal left the antenna and entered the ground, ensuring accurate positioning of surface reflections. Second, antenna coupling removal was carried out to mitigate interference between the transmitter and receiver, along with reducing ringing noise and excessive reflections, by effectively subtracting the background signal. Finally, noise was suppressed and hidden patterns within the data were revealed, significantly improving overall signal quality, by using a band-pass filter tailored to the GPR system operating frequency range of 1.2 GHz to 2.8 GHz.

2) Holographic Radar Tomography: In a healthy tree, moisture is evenly distributed throughout the trunk, increasing gradually from the outer bark toward the inner core, with typical moisture content ranging between 35% and 60% [7]. The balanced distribution is critical for nutrient transport and structural stability, maintaining the vitality and strength of the tree. The dielectric properties of the wood can be significantly affected by any disruption, such as decay or hollowing, indicating changes in the structural integrity of the tree. Valuable insights into the internal health of the tree are provided by monitoring these variations, aiding arborists and researchers in preservation efforts. Using holographic radar tomography, as outlined by (7), significant improvements in signal-to-noise ratio (SNR) have been achieved, enabling clear detection of reflections deep within the trunk, up to 15 ns. These results, illustrated in Figure 5 with HH and VV component B-scans, demonstrate a far greater depth of observation than traditional ground-penetrating radar methods. The method proposed in this study addresses these challenges by incorporating a processing strategy grounded in physical principles. It not only enhances SNR but also accurately highlights areas with significant changes in relative permittivity valuue, providing more dependable and meaningful insights.

3) Kichoof Migration: Traditional Kirchhoff migration in GPR involves tracing EM reflections from the subsurface to their origin by calculating the travel time of waves from the transmitter to the receiver and then back-propagating them to the inner structures. The arc-shaped Kirchhoff migration method enhances this process by incorporating curved survey paths, which improves image accuracy and resolution, especially in complex subsurface regions. This approach is particularly beneficial for tree trunk inspections, as it provides clearer images of internal structures, helping identify critical features in diseased trees. In this method, the relative permittivity (ε_r) of the tree trunk is set to 20 based on moisture content and weather conditions, enabling 3D image reconstruction. The imaging aperture is chosen as 90° based on the radiation pattern of the antenna and the shape of the tree, with an azimuth angle of 1°, radial resolution of 0.25 cm, and vertical resolution of 1 cm. Detailed insights into the internal structure of the tree are provided by the resulting 3D images, which are discussed in the following section.

C. *Results and Discussions*

The results presented in Figure 6 provide a detailed visualization of the reconstructed sections extending from the base to the top of the analyzed tree trunk. Careful analysis reveals distinct internal patterns, offering valuable insights into the structural characteristics and internal dynamics of the trunk. One of the most prominent features revealed by the reconstruction is the presence of high-energy regions, which

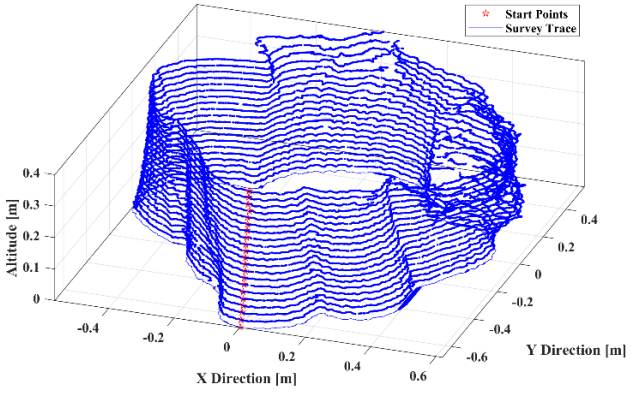

Fig. 4. GPR survey traces extracted from 3D model generated using SfM technique.

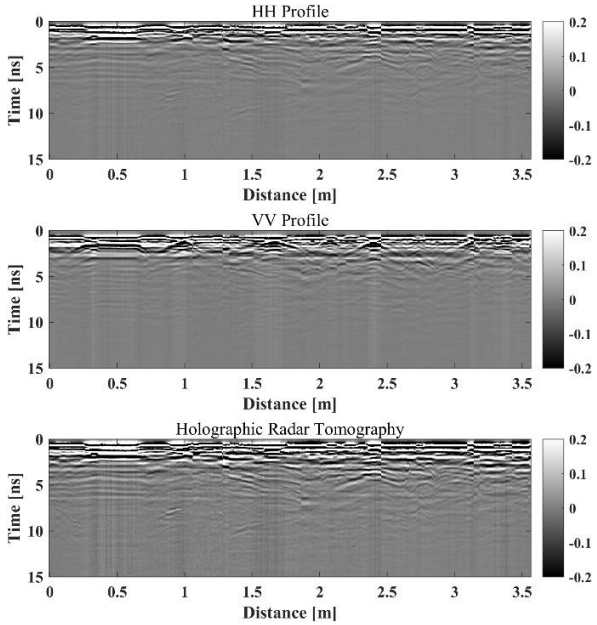

Fig. 5. B-scans of tree trunk before and after holographic radar tomography processing.

serve as clear indicators of internal anomalies within the trunk. Figures 7(a) and 8(a) provide perspective views illustrating the high-energy regions within the examined trunk, displayed in a three-dimensional representation. The actual photographs of the tree are shown in Figures 7(b) and 8(b), providing valuable insights into the health of tree trunk and structural integrity. In Figure 7(a), a prominent feature is visible, extending from the base of the trunk and covering nearly the entire height of the examined section. Notably, this feature corresponds closely to a bark discoloration seen in Figure 7(b). The alignment between the high-energy region in the 3D rendering and the observed anomaly in the photograph validates the accuracy of the reconstruction process, as seen in the side view. Moving on to Figure 8(a), a significant feature extending throughout the trunk on this side is prominently visible in the upper portion of the image. Upon closer inspection, it becomes apparent that this feature aligns seamlessly with the dark bark region in Figure 8(b).

The comprehensive analysis of the results reveals several key insights into the health and integrity of tree trunk. First, clear evidence of a fungal infection extending from the bark

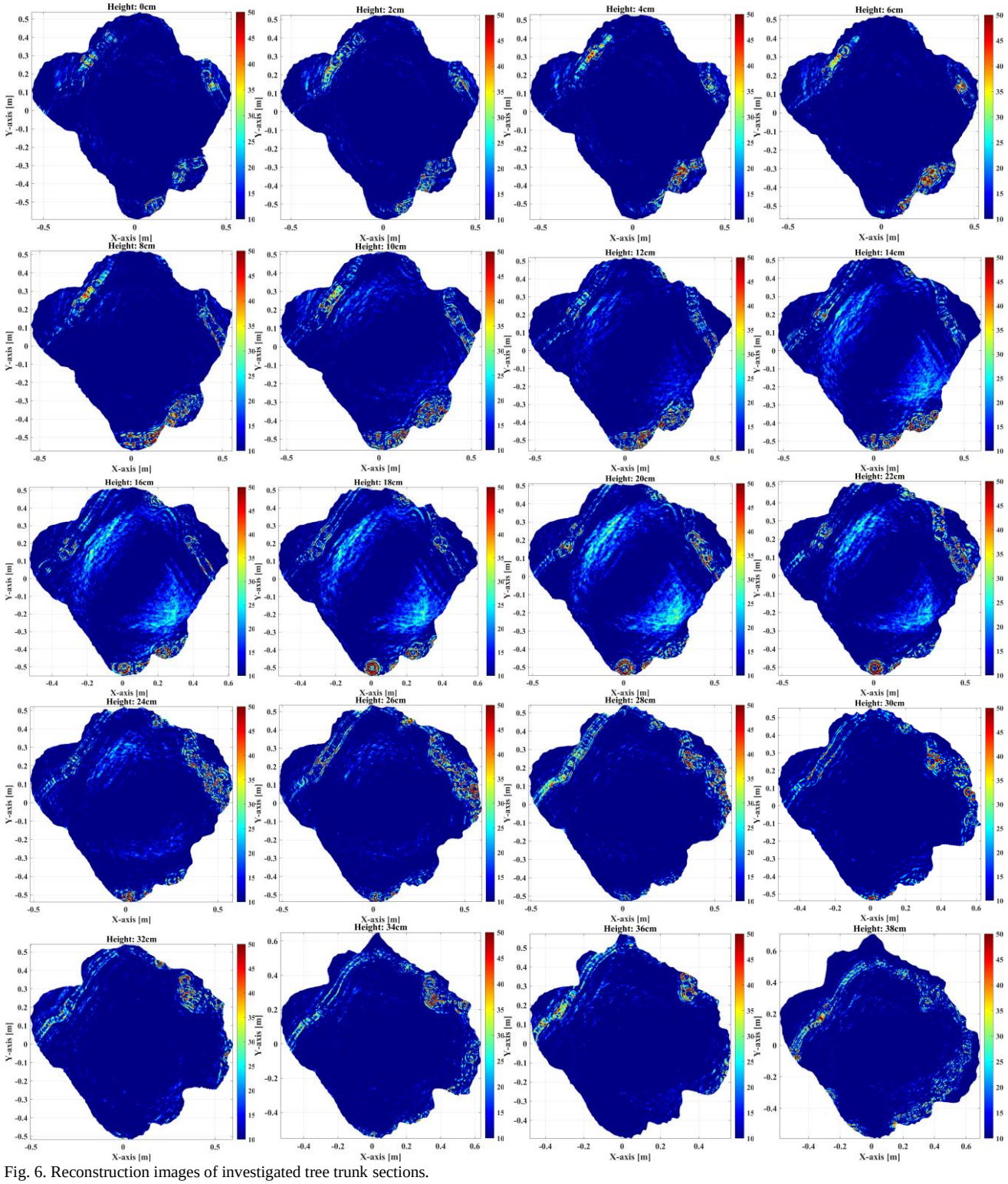

Fig. 6. Reconstruction images of investigated tree trunk sections.

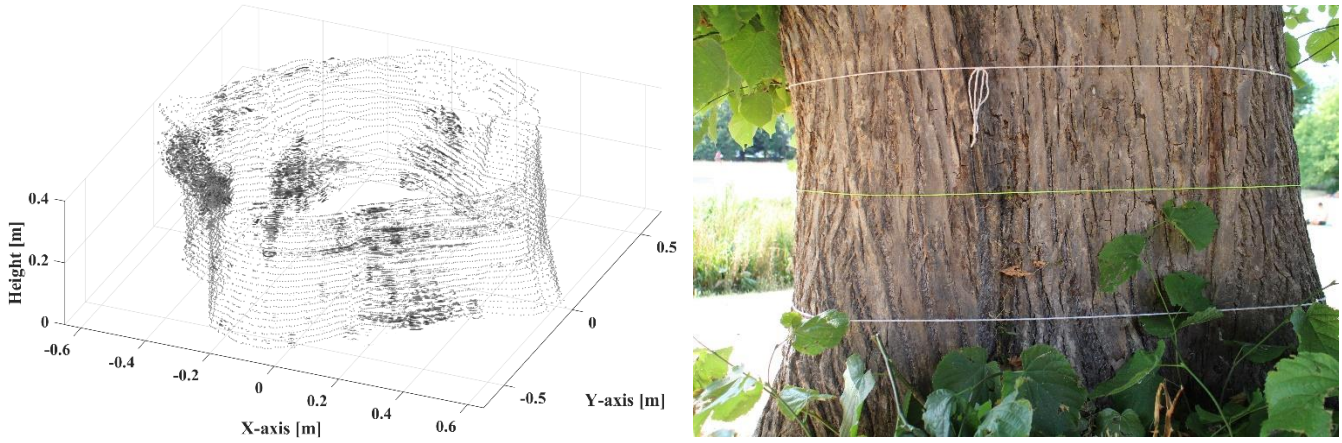

(a) (b)

Fig. 7. Reconstruction 3D images and real photograph of investigated tree trunk.

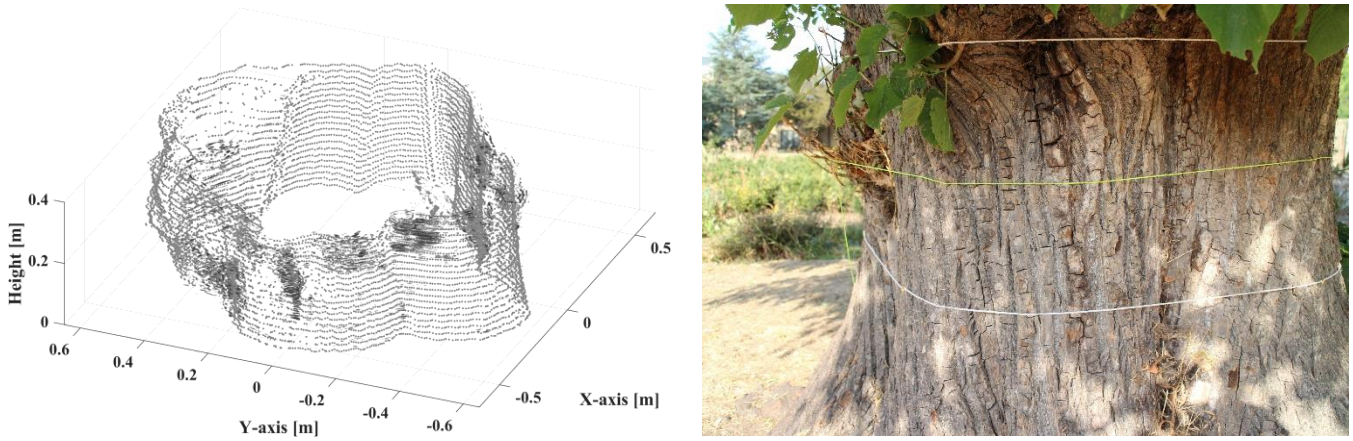

(a) (b)

Fig. 8. Reconstruction 3D images and real photograph of investigated tree trunk.

to the interior of the tree is indicated by the alignment of high-energy areas with structural anomalies. Second, the absence of internal hollows suggests that the overall structural integrity of tree trunk remains largely intact. However, despite the minimal current impact on structural stability, the fungal infection warrants regular monitoring to track its progression and evaluate any potential risks to the long-term health of live tree.

IV. Conclusions

In this study, a set of signal processing methodologies was developed to assess trunk health using GPR. The primary objective was to detect early signs of decay and small cavities, enabling timely interventions to prevent pruning or tree removal. However, the complex structure, electromagnetic properties, and irregular shapes of living trees posed challenges for traditional GPR techniques. To address these, a novel approach was proposed, integrating structure-from-motion photogrammetry, holographic radar tomography, and Kirchhoff migration. SfM photogrammetry was utilized to reconstruct the three-dimensional shape of the trunk, ensuring precise positioning of the GPR operating track. Holographic radar tomography was developed to enhance signal quality by combining HH and VV polarization reflections. Finally, the Kirchhoff migration algorithm was applied to account for trunk irregularities. This integrated framework, validated through real measurements, provided detailed internal and external imaging, advancing tree health monitoring and supporting environmental and cultural conservation.

References

[1] D. Feurer and F. Vinatier, “Joining multi-epoch archival aerial images in a single SfM block allows 3-D change detection with almost exclusively image information,” ISPRS J. Photogramm. Remote Sens., vol. 146, pp. 495-506, December 2018.

[2] S. Jiang, C. Jiang and W. Jiang, “Efficient structure from motion for large-scale UAV images: A review and a comparison of SfM tools,” ISPRS J. Photogramm. Remote Sens., vol. 167, pp. 230-251, Sepember 2020.

[3] L. Zou, H. Liu, A. M. Alani and G. Fang, “Surface Permittivity Estimation of Southern Utopia Planitia by High-Frequency RoPeR in Tianwen-1 Mars Exploration,” IEEE Trans. Geosci. Remote Sens., vol. 62, pp. 1-9, Feburary 2024, Art no. 2002809.

[4] S. Lambot and F. André, “Full-wave modeling of near-field radar data for planar layered media reconstruction,” IEEE Trans. Geosci. Remote Sens., vol. 52, no. 5, pp. 2295-2303, May 2013.

[5] A. De Coster and S. Lambot, “Full-wave removal of internal antenna effects and antenna–medium interactions for improved ground-penetrating radar imaging,” IEEE Trans. Geosci. Remote Sens., vol. 57, no. 1, pp. 93-103, July 2018.

[6] L. Zou, F. Tosti and A. M. Alani, "Nondestructive Inspection of Tree Trunks Using a Dual-Polarized Ground-Penetrating Radar System," IEEE Trans. Geosci. Remote Sens., vol. 60, pp. 1-8, June 2022.

[7] C. Skaar, Wood-water relations. Springer Science & Business Media, 2012.